

Polariton Reflectance and Photoluminescence in High-Purity GaAs

D. D. Sell, S. E. Stokowski,* R. Dingle,† and J. V. DiLorenzo

Bell Laboratories, Murray Hill, New Jersey 07974

(Received 7 November 1972)

The low-temperature optical reflectance and photoluminescence of high-purity GaAs have been studied in the spectral energy region near the direct fundamental gap. Strong free-exciton reflectance structure is seen. This structure is strongly influenced by both spatial dispersion and polariton effects. The general shape and strength of this reflectance structure are well accounted for by polariton theory with the unknown surface-barrier thickness as the only adjustable parameter. The sharp spike in the reflectance data provides an accurate value $E_L = 1.51515 \pm 0.00015$ eV for the longitudinal exciton energy at 2 K. The longitudinal-transverse exciton splitting falls within the range 0.1–0.25 meV. Two structures in the luminescence spectrum are interpreted, respectively, as lower (LPB) and upper polariton branch (UPB) luminescence. The LPB luminescence occurs at the transverse exciton energy as expected. The UPB luminescence, previously identified as the “free-exciton” structure, has the rather unusual behavior that it always occurs above, and has its low-energy “onset” at, the longitudinal exciton energy. Uniaxial stress and temperature-dependence results are presented to support the interpretation of the data. The over-all energy splittings and polarization behavior seen in both reflectance and luminescence spectra agree with theoretical results. The stress behavior of the reflectance provides the value $j = -0.05 \pm 0.05$ meV for the exciton exchange energy. An anticrossing seen in the piezoluminescence data is attributed to an interaction, arising from the valence-band anisotropy, of the UPB with an optically forbidden triplet exciton state. Possible alternative explanations of the luminescence data are discussed and comparisons are made with earlier work.

I. INTRODUCTION

Recently, the authors have published a brief account¹ (hereafter referred to as I) of polariton reflectance and luminescence studies in high-purity GaAs. In this paper we present a detailed discussion of these results. We focus our attention upon the free exciton and consider bound-exciton spectra only to the extent that these bound-exciton features help us to understand the free-exciton behavior. (We use the terms free exciton and polariton nearly interchangeably. The term polariton is used where it is important, or necessary, to emphasize the exciton-photon interaction.)

Historically, much attention has been given to the optical properties of GaAs near the fundamental band edge. GaAs is of interest both because of its use in devices and because in many respects it is a “model” direct-band-gap semiconductor. Simple theoretical models (such as the hydrogenic-exciton theory) often give a reasonably good account of the actual behavior of GaAs.

Much of the work on the direct-gap optical properties of GaAs has been directed toward luminescence studies. The extent of this luminescence literature is indicated in the review by Williams and Bebb.² Most of this work has been concerned with extrinsic luminescence. Weak intrinsic luminescence has been seen in recent years only in moderately pure material. Even in high-purity material, the impurity-induced luminescence still dominates the spectrum.

Transmission and reflectance spectra near the

band edge have received much less attention.

There is the early work of Sturge³ which beautifully demonstrated the importance of exciton effects in the absorption spectrum. Sturge’s material was impure ($\sim 10^{17}$ impurities/cm³) by present standards and discrete exciton lines were not resolved.

Recently, as a part of the present reexamination of the GaAs spectrum, Sell⁴ resolved the $n=1$ and 2 exciton transitions in high-purity material and obtained the value 4.2 ± 0.2 meV for the exciton binding energy. Hill⁵ has confirmed these results.

The reflectance spectrum has received very little attention. Prior to this work, the only direct-reflectance measurements (on relatively pure material) were those by Shay and Nahory,⁶ who were not able to interpret their data (in part because earlier luminescence results led them to believe that they were seeing bound-exciton transitions). Various modulation techniques have been used to study $\delta R/R$ in this spectral region but generally these results suffer from at least one of two shortcomings: (1) Impure samples ($>10^{16}$ cm⁻³) were used. (2) There is inherent difficulty in interpreting modulation data. In either case such studies have had limited success in establishing the fundamental optical properties at the band edge in GaAs.

In general, our results indicate that this shunning of reflectance (and absorption) spectroscopy in favor of luminescence work was not warranted. We feel that our progress in understanding all of these spectra was advanced by carefully comparing the complementary information obtained from reflectance, luminescence, and transmittance spec-

tra. The reflectance studies, in particular, have been of central importance in developing our interpretation of these spectra. For the high-purity material used in this work, the reflectance and transmittance spectra are dominated by intrinsic rather than extrinsic characteristics. In contrast, the luminescence spectrum is still strongly affected by impurity-related effects. Similarly, the theory for polariton reflectance and absorption is relatively simple and developed compared with that for luminescence which is not sufficiently developed to permit a quantitative comparison with experiment.

II. OUTLINE OF PAPER AND SUMMARY OF RESULTS

In this paper we have tried to give a full account of our investigation to permit others to make independent evaluations of the experimental results and our interpretation of these data. This has necessarily resulted in a lengthy manuscript which deals with a variety of topics. In this section we provide an outline of the paper and briefly summarize our main results.

Section III gives various experimental details concerning the apparatus, the photon energy calibration and accuracy, and the sample growth and characteristics. In Sec. IV, the polariton-spatial-dispersion theory is used to calculate the exciton reflectance for both nondegenerate and degenerate exciton bands. The reflectance data are presented in Sec. V and are compared with the calculated polariton reflectance. The luminescence results are presented in Sec. VI and a model for the free-exciton luminescence involving both upper- and lower-branch polaritons is proposed. Stress results for both reflectance and luminescence spectra are given in Sec. VII and are compared with the calculated behavior. The temperature dependence of the luminescence and the role of excited exciton states are briefly discussed in Secs. VIII and IX, respectively.

One main result is that we have observed and have carefully studied the characteristic reflectance spectrum for the $n=1$ free exciton. This reflectance has a strongly "nonclassical" spectral shape which, for increasing photon energy, consists of a small positive slope, a strong minimum, a weak sharp spike seen for some, but not all, samples, and finally a flat reflectance. This reflectance spectrum is identified with the $n=1$ free exciton by the following evidence: (a) It is coincident in energy with a strong absorption line which has the expected behavior for an $n=1$ exciton transition. (b) The observed shape and amplitude of this characteristic reflectance are well accounted for by the polariton-spatial-dispersion theory. (c) No reflectance structure is seen at energies corresponding to known bound exciton lines. Together with the preceding points, this rules out the possibility that

the reflectance is impurity related. (d) The structure exhibits the expected stress behavior.

According to the polariton theory, the sharp spike seen at 1.51515 ± 0.00015 eV at 2 K occurs at the longitudinal exciton energy, and the minimum in the reflectance occurs near the transverse exciton energy. The experimental energy separation between the reflectance spike and the minimum is 0.25 meV compared with a theoretical value of 0.1 meV for the longitudinal-transverse exciton splitting. The observed stress dependence of the reflectance gives a value $j = -0.05 \pm 0.05$ meV for the exciton exchange constant.

The second main result is that we have observed exciton luminescence near the free-exciton energy, similar to previous work, but present a new interpretation of the spectrum. We associate two lines with free-exciton luminescence. The key point is that the luminescence previously identified as the "free-exciton" line occurs above the longitudinal exciton energy and has its low-energy "onset" at this energy. We identify this structure with upper-polariton-branch (UPB) luminescence. A second luminescence line, previously assumed to be a bound exciton transition, occurs at the transverse exciton energy. On the basis of its energy and its temperature dependence, it is identified as the lower-polariton-branch (LPB) luminescence. These interpretations are supported by stress and temperature dependence results, and by comparison with theory.

III. EXPERIMENTAL DETAILS

A. Reflectance Apparatus

The reflectance data were obtained with a double-beam spectrophotometer described previously.⁷ A 75-W xenon arc lamp was focused onto the entrance slit of a 1-m Czerny-Turner Jarrell-Ash monochromator (8 Å/mm dispersion) through a 2-64 Corning filter. For the polarized-stress experiments, a Glan-Thompson polarizer was located at the entrance slit of the monochromator. A refracting chopper was used to alternately illuminate an aluminum reference mirror (located outside the sample Dewar) and the sample. The two light beams were superimposed at the photocathode of an EMI 9659QA photomultiplier tube with a toroidal mirror. The ratio of the sample and reference signals was taken electronically, stored in a multi-channel analyzer, and punched onto paper tape. Finally, a digital computer was used to perform the wavelength-energy conversion for each data point, to scale the data (to account for the actual reflectance of the reference mirror and the transmission losses of the Dewar windows), and to plot the results.

The samples were immersed in pumped liquid

helium in a Janis "Super Vari-Temp" metal Dewar. Since these sharp spectra are especially sensitive to strain, the samples must be mounted carefully so that unwanted strains are not introduced as the sample is cooled. Generally we attached the sample to a copper sample holder with only one small drop of rubber cement applied at one corner. If the sample is inadvertently stressed, the spectra exhibit obvious symptoms: The reflectance peak splits or broadens, and in addition, such effects are more noticeable near the spot where the sample is glued to the holder.

B. Wavelength Calibration and Wavelength-Energy Conversion

Since small differences of a few tenths of a millivolt are significant in the interpretation of these spectra, the wavelength calibration and the wavelength-energy conversion are both important. For calibration we have used the atomic mercury line at 4077.83 Å in second order to obtain an air-wavelength calibration at 8155.7 Å in the spectral region under study. Using recently compiled values of the fundamental constants,⁸ the air wavelength (Å) to energy (eV) conversion is

$$E = \frac{hc}{n_a \lambda_a} = \frac{12398.54}{n_a \lambda_a}, \quad (3.1)$$

where n_a is the refractive index of air. In our computerized data analysis, n_a is calculated for each data point from Edlén's formula⁹; however, n_a is essentially constant at the value 1.0002749 in the spectral region near 1.5 eV and Eq. (3.1) becomes

$$E = 12395.13/\lambda_a. \quad (3.2)$$

The wavelength-energy conversion factor (1.23944 eV/μm) given by Bimberg and Schairer¹⁰ and Evangelisti *et al.*¹¹ differs from this result by less than 0.1 meV.

Our absolute accuracy and day-to-day reproducibility for the photon energy are better than 0.1 meV.

C. Luminescence and Single-Beam Reflectance Apparatus

Figure 1 illustrates the optical apparatus for the luminescence and the combined reflectance-luminescence experiments. With the exception of the auxiliary tungsten lamp, this is a conventional luminescence apparatus. The helium-neon laser power at 6328 Å was approximately 30 mW in multimode and approximately 7 mW in single-transverse-mode operation. Generally the laser illuminated a spot on the sample a few millimeters in diameter and this spot was imaged onto the entrance slit of the spectrometer. In this configuration, the laser pump intensity was reasonably uniform and could be estimated from the measured beam area and power. The pump intensity could

be controlled with neutral density filters or by varying the laser-beam area.

With the tungsten lamp included, this apparatus could also be used for conventional single-beam specular reflectance measurements. This single-beam-reflectance apparatus is considerably inferior to the double-beam apparatus described in Sec. III A, but it has the important advantage that direct and accurate comparisons can be made between the reflectance and luminescence spectra. With the laser and the lamp illuminating a common area of the sample the following experiments can be performed: (a) ordinary reflectance (laser off), (b) ordinary luminescence (lamp off), and (c) reflectance as a function of laser pumping power. The approach overcomes two problems encountered in less direct comparisons of reflectance and luminescence. First, a given area of the sample is studied in all three measurements, thereby eliminating any difficulty of sample-to-sample variations. Second, any ambiguities caused by spectrometer calibration are removed because the same instrument is used for all three measurements which can be performed in rapid succession. For the combined reflectance-luminescence data, the relative energy calibration uncertainty is less than 0.05 meV.

The early luminescence measurements in this study were performed with a separate apparatus from that used for the double-beam reflectance measurements. A cooled RCA 7102 photomultiplier tube and a second 1-m Jarrell-Ash Czerny-Turner spectrometer were used. The later luminescence and combined reflectance-luminescence studies were performed with the same apparatus (and spectrometer) used for the double-beam reflectance work.

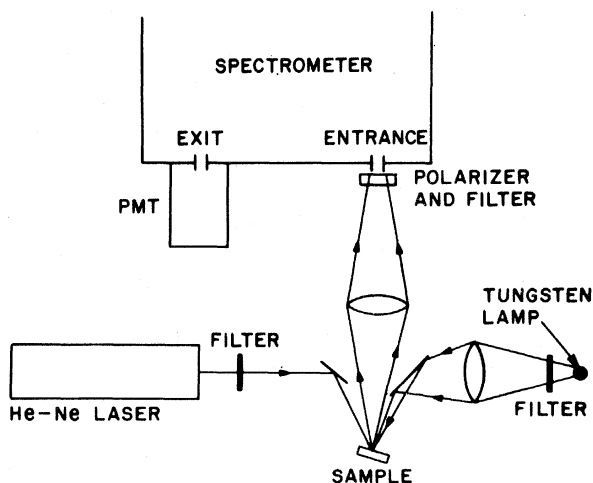


FIG. 1. Apparatus for photoluminescence and single-beam reflectance.

D. Stress Apparatus

Different stress apparatus were used for the reflectance and luminescence stress experiments. For the reflectance studies, the stress apparatus was very similar to that shown in Fig. 1 of Ref. 12 except for the following: (a) No sample mounting cap was used. Instead, the sample was supported on a pedestal with double-sided tape and a piece of paper was used for a cushion on the top of the sample. (b) The sample was immersed in pumped liquid helium. (c) The force was applied to the plunger directly with calibrated weights. The stress apparatus for the luminescence was quite similar except that it was designed to be mounted into a quartz cryostat and the sample was cooled to approximately 5 K by a flow of cold helium gas. The samples (substrate plus epitaxy) were approximately $0.5 \times 1.0 \times 8$ mm rectangular parallelepipeds with the long axis oriented along the $\langle 001 \rangle$ or $\langle 110 \rangle$ crystallographic directions. For such sample cross sections we could conveniently apply stresses in the range 50–4000 kg cm⁻². The 0.5-mm dimension, imposed by the substrate thickness, is rather thin. This causes some difficulty with sample bending which in turn causes some uncertainty in the actual applied stress at the sample surface. Consequently we do not attempt to extract accurate values for the deformation potentials from our results.

E. Samples

The samples were epitaxial layers of GaAs grown on GaAs by chemical vapor deposition using the AsCl₃/Ga/H₂ system. The high purity of the samples was obtained by properly choosing the substrate orientation, substrate temperature and pressure of AsCl₃ in the system. The complete details of the process have been presented elsewhere.¹³

Table I lists the properties of several epitaxial films for which data are reported in this paper. The values of the mobility at room temperature and 77 K were determined by Hall measurements using the van der Pauw¹⁴ technique. The samples

had values of the free-carrier concentration in the range $(1-7) \times 10^{13}$ cm⁻³, and mobilities at 77 K in the range 150 000–200 000 cm²/V sec. The values of the total ionized impurity concentration $N_D + N_A$ are in the range $(1.5-6) \times 10^{14}$ cm⁻³. The $N_D + N_A$ values were obtained using the recent calculations of Rode and Knight.¹⁵

In general, these samples are among the purest GaAs presently available. In this paper we use the term "high-purity" to mean (*n*-type) material with $\mu_{77} > 100\,000$ cm²/V sec (and *p*-type material of comparable purity). We find that, with the possible exception of some differences in linewidths, all samples meeting this criterion exhibit the same general reflectance and luminescence spectra. Although most of our work has been carried out on $\{001\}$ faces of the *n*-type vapor-phase epitaxial material described above, we have confirmed that the same reflectance and luminescence behavior is also seen for comparably grown $\{211\}A$ and $\{311\}A$ and *B* orientations, for *n*-type liquid-phase-epitaxial material (kindly provided by Hwang), and for *p*-type material (same reflectance, but different luminescence) grown by molecular-beam epitaxy (kindly provided by Wiegmann and Tracy).

IV. POLARITON-SPATIAL-DISPERSION THEORY

A. Simple Nondegenerate Bands

In this section we apply the polariton-spatial-dispersion theory of Hopfield and co-workers^{16,17} to the case of the free exciton in GaAs. Two distinct effects are included. First, the exciton-photon interaction requires that the true normal modes of the system, referred to as polaritons, be admixtures of exciton- and photon-like states. In the region near the intersection of the original exciton and photon dispersion curves, the admixture is large. The exciton-photon interaction causes an energy splitting between the longitudinal and transverse polaritons. Second, spatial dispersion, as we use the term here, refers to the fact that the original exciton energy is a function of \vec{K} due to the "center-of-mass" motion of the

TABLE I. Properties of the samples for which data are presented. All samples are *n*-type and were grown by vapor phase epitaxy.

Sample	Orientation	Thickness (μm)	μ_{77} cm ² /V sec	n_{77} (cm ⁻³)	μ_{300} (cm ² /V sec)	n_{300} (cm ⁻³)
S-32	$\{311\}A$	54	150 000	7.3×10^{13}	9050	7.0×10^{13}
S-39	$\{100\}$	20	183 000	2.8×10^{13}	8820	2.5×10^{13}
S-40	$\{100\}$	69	199 000	4.4×10^{13}	8760	4.8×10^{13}
S-41	$\{100\}$	52	173 000	5.0×10^{13}	8760	5.0×10^{13}
S-59	$\{100\}$	40	163 000	1.0×10^{13}	8870	8.6×10^{12}
S-61	$\{100\}$	56	174 000	4.5×10^{13}	8830	4.6×10^{13}
S-62	$\{100\}$	59	167 000	2.2×10^{13}	8420	1.9×10^{13}

exciton. For simple nondegenerate electron and hole bands the exciton dispersion relation is

$$E_{\text{ex}}(K) = E_0 + \frac{\hbar^2 K^2}{2M^*}, \quad (4.1)$$

where $M^* = m_e^* + m_h^*$ is simply the total mass of the exciton. For the case of degenerate bands the situation is somewhat more complicated as discussed below; however, the resulting reflectance is essentially the same as for the nondegenerate case.

With spatial dispersion, it is possible to have two propagating modes in the crystal as discussed by Hopfield and Thomas¹⁶ (HT). This introduces an additional boundary condition which can have a rather dramatic effect upon the reflectance spectrum. Following HT, we take the surface boundary condition to be the case in which the exciton is excluded from a layer of thickness l at the surface¹⁸; then the reflectance is given by

$$R = \left| \frac{1 - n^*}{1 + n^*} \right|^2, \quad (4.2)$$

where

$$n^* = n \left[\frac{(n^\dagger + n) e^{-i\theta} + (n^\dagger - n)}{(n^\dagger + n) e^{-i\theta} - (n^\dagger - n)} \right], \quad (4.3)$$

$$\theta = 2knl, \quad (4.4)$$

and

$$n^\dagger = (n_1 n_2 + \epsilon_0) / (n_1 + n_2). \quad (4.5)$$

Here ϵ_0 is the (assumed) energy-independent background dielectric constant in the spectral region of interest, $n = (\epsilon_0)^{1/2}$, k is the wave vector of the incoming photon, θ is the phase lag for a two-way traversal of the boundary layer, n^\dagger is the "effective" index of the medium including the excitons, and n_1 and n_2 are the two complex refractive indices for the two branches of the polariton dispersion as given by Eq. (11) of Ref. 16.

To obtain theoretical reflectance curves for comparison with experiment we use these results of HT and choose values for the five parameters ϵ_0 , M^* , β (polarizability), θ , and Γ (broadening) appropriate for GaAs. The values for ϵ_0 , M^* (discussed below), and β (see Sec. VB) are known and are given in Table II. The sharp "spike" in the reflectance data indicates that the broadening parameter Γ is usually negligibly small (at 2 K). Thus, only the surface boundary layer phase θ remains as an adjustable parameter in the theory. In Fig. 2 we illustrate the theoretical polariton reflectance curves for GaAs for values of θ in the range from 0 to 2π . The surface barrier obviously has a strong effect upon the reflectance. As discussed below in Sec. V, the best agreement with experiment is obtained for $\theta \sim 90^\circ$.

B. Degenerate Bands

Before we attempt a comparison with the data we must account for the fact that the excitons in GaAs are not simple nondegenerate bands, and must determine the value of the exciton mass M^* . Owing to the light-heavy-hole degeneracy of the valence bands, there are two exciton branches which are degenerate at $\vec{k} = 0$, but which (in general) have different anisotropic masses. Kane¹⁹ has shown that to second order in the d -like valence-band Hamiltonian, the effective masses for the two exciton bands are given by

$$\frac{1}{M_{\text{eff}}} = \frac{1}{m_e^* + m_h^*} - \gamma_h^2 \mu_0 \left(\frac{1}{2\mu_2^2} + \frac{4}{\mu_1^2} \right) \pm \gamma_h^2 \left[\frac{4}{\mu_1^2} + \left(\frac{1}{\mu_2^2} - \frac{12}{\mu_1^2} \right) \left(\frac{K_x^2 K_y^2 + K_x^2 K_z^2 + K_y^2 K_z^2}{K^4} \right) \right]^{1/2}, \quad (4.6)$$

where

$$\gamma_h = \frac{m_h^*}{m_e^* + m_h^*}, \quad (4.7)$$

TABLE II. Parameters for GaAs.

Values	Comments
$\epsilon_s = 12.56 \pm 0.4^a$	Static dielectric constant
$\epsilon_0 = 12.6^b$	Background dielectric constant near 1.51 eV
$m_e^* = 0.06650 \pm 0.00007^a$	
$\gamma_1 = 7.2 \pm 0.6^c$ $= 7.65^d$	
$\gamma_2 = 2.5 \pm 0.4^c$ $= 2.41^d$	Luttinger parameters
$\gamma_3 = 2.9 \pm 0.3^c$ $= 3.28^d$	
$m_h^* = m_0 / \gamma_1 = 0.131 m_0$	"Isotropic" hole mass
$\mu_0 = 0.044 m_0$	$\mu_0^{-1} = m_e^{*-1} + m_h^{*-1}$
$\mu_1 = m_0 / \gamma_2 = 0.415 m_0$	
$\mu_2 = m_0 / 2(3)^{1/2} \gamma_3 = 0.088 m_0$	
$M^* = 0.298 m_0$	Total exciton mass
$4\pi\beta = 1.6 \times 10^{-3}$	Exciton polarizability
$R_0^* = 4.2 \pm 0.2 \text{ meV}^e$	$n=1$ free-exciton binding energy
$r = 136 \text{ \AA}$	$n=1$ free-exciton radius

^aG. E. Stillman, D. M. Larsen, C. M. Wolfe, and R. C. Brandt, *Solid State Commun.* **9**, 2245 (1971).

^bEstimated from B. O. Seraphin and H. E. Bennett, *Semiconductors and Semimetals*, edited by R. K. Willardson and A. C. Beer (Academic, New York, 1967), Vol. 3, p. 499.

^cAn average of the experimental values tabulated by M. Reine, R. L. Aggarwal, and B. Lax, and C. M. Wolfe, *Phys. Rev. B* **2**, 458 (1970); by A. L. Mears and R. A. Stradling, *J. Phys. C* **4**, L22 (1971); and the semiempirical values of Lawaetz, Ref. 21.

^dLawaetz, Ref. 21.

^eSell, Ref. 4.

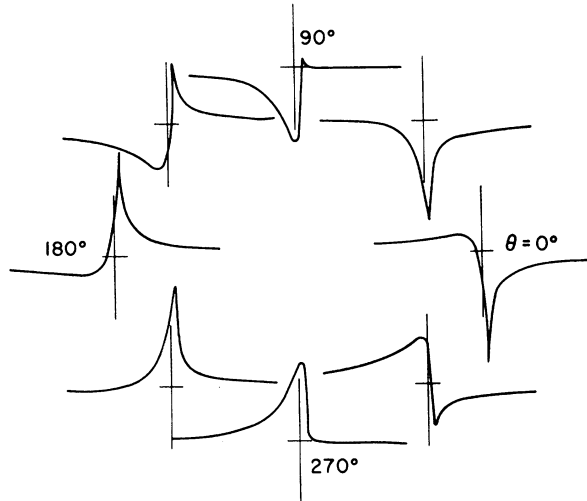


FIG. 2. Calculated polariton reflectance for the parameters $\epsilon_0=12.6$, $M^*=0.298m_0$, $4\pi\beta=1.6 \times 10^{-3}$, $\Gamma=0$, and $\theta=2knl=0^\circ, 45^\circ, 90^\circ, 135^\circ, 180^\circ, 225^\circ, 270^\circ$, and 315° (corresponding to a surface layer thickness in the range 0–1150 Å). For each spectral trace the vertical fiducial mark represents the transverse exciton energy [E_0 of Eq. (4.1)] and the horizontal mark indicates the background reflectance $R = |(n-1)/(n+1)|^2 = 0.314$. For θ in the range 90° – 180° , the positive spike occurs at the longitudinal exciton energy E_L . For θ in the fourth quadrant (270° to 0°), the negative peak occurs at E_L .

and m_h^* , μ_0 , μ_1 , and μ_2 are defined in terms of the Luttinger parameters by Baldereschi and Lipari²⁰ as shown in Table II. For degenerate bands, the dispersion curve (4.1) is replaced by

$$E_{\text{ex}}^*(\vec{K}) = E_0 + \frac{\hbar^2 K^2}{2M^*} [1 \pm \gamma(\hat{K})], \quad (4.8)$$

where M^* is defined by

$$\frac{1}{M^*} = \frac{1}{m_e^* + m_h^*} - \gamma_0^2 \mu_0 \left(\frac{1}{2\mu_2^2} + \frac{4}{\mu_1^2} \right), \quad (4.9)$$

and has the value $M^*=0.298$ using Lawaetz's semiempirical values for the Luttinger parameters²¹ (see Table II).

In Eq. (4.8), $\gamma=0.63$ for \vec{K} parallel to $\langle 100 \rangle$ and $\gamma=0.86$ for \vec{K} parallel to $\langle 111 \rangle$. We have calculated the polariton reflectivity for the case of isotropic bands ($\gamma=\text{constant}$). This problem (three propagating modes in the crystal rather than two) is essentially the same as that considered by Mahan and Hopfield²² for exciton bands split by a linear- K term. Their analysis can be followed almost exactly for the present problem if we simply replace their linear- K term by a term quadratic in K . We have calculated the reflectance spectrum for various values of γ and find that the reflectance curves are substantially the same as those for the nondegenerate case ($\gamma=0$). Figure 3 illustrates that the general shape of the reflectance spectrum

is not sensitive to the value of γ ; however, the amplitude of the structure increases somewhat as γ increases. Figure 3 also demonstrates that a small broadening, $\Gamma=0.05$ meV, can have a considerable effect upon the strength of the negative peak. Since it is not our purpose to make a detailed fit between theory and experiment, it is adequate to note that no qualitatively new features are introduced by the degeneracy. For semiquantitative comparisons with experiment we are justified in using the theoretical results for the nondegenerate case.

V. REFLECTANCE RESULTS

A. Data and Comparison with Theory

Figure 4 presents six reflectance spectra at 2 K which illustrate several features of the data characteristic for high-purity material. Several sample properties are given in Table I. All of these spectra except curve (f) were obtained on as-grown surfaces. More than twenty high-purity samples have been studied. Most as-grown samples exhibit the general spectral shape seen in curves (a), (b), (c), (d), and (f). There are important differences in these five spectra which are discussed below, but all have the same general spectral shape. The remaining few samples exhibit features similar to curve (e). The spectral curves (e) and (f) were obtained on the same sample S-59: Curve (e) is for the as-grown surface; curve (f) was obtained after the sample had been chemically polished in a dilute solution of bromine in methanol. On the other hand, the samples which initially exhibited spectra similar to curves (a)–(d) retained the same spectral shape after an identical polishing procedure. Although much of our work has been done on $\{001\}$

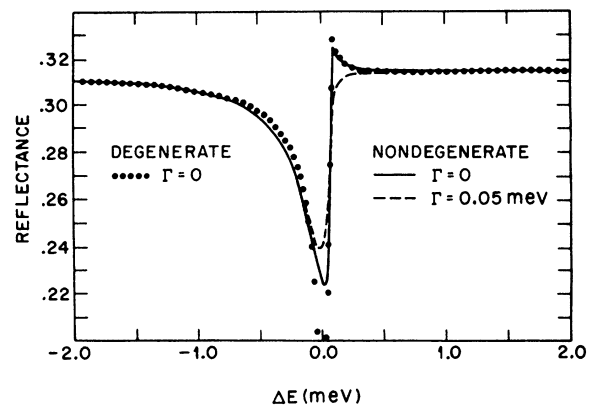


FIG. 3. Comparison of the polariton reflectance calculated for simple nondegenerate bands (solid line, $\Gamma=0$; dashed line, $\Gamma=0.05$ meV) with that calculated for the case of degenerate valence bands (dotted curve, $\Gamma=0$ and $\gamma=0.75$). For all curves, $\theta=90^\circ$. The minimum of the dotted curve is off scale at 0.17.

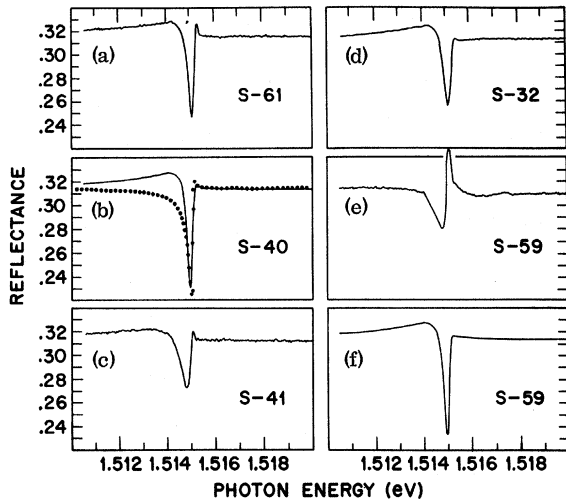


FIG. 4. Tracings of near-normal-incidence reflectance data at 2 K for six high-purity samples. Spectra (a) through (e) were obtained on as-grown surfaces; the sample for spectrum f has been chemically polished. All samples have $\{100\}$ faces except S-32 [in (d)] which has a $\{311\}A$ face. The samples S-61 and S-41 in spectra (a) and (c) exhibited a lower background reflectance and some nonspecular scattering due to surface roughness. To account for this and to permit direct comparisons with other data, these data in (a) and (c) have been multiplied by the factors 1.25 and 1.32, respectively, to bring the background reflectance up to the theoretical value of 0.314.

surfaces, we have also studied $\{211\}A$, $\{311\}A$, and $\{311\}B$ orientations. In general the results for these orientations are the same as for the $\{001\}$ face as illustrated in curve (d) for the $\{311\}A$ face. We conclude from these observations that the general spectrum in curves (a), (b), (c), (d), and (f) is the "characteristic" reflectance spectrum for a clean (but air exposed) free surface of high-purity GaAs. The common features of this "characteristic" spectrum are (a) a small positive slope (dR/dE) for photon energies below the exciton energy, (b) a strong, relatively sharp minimum in the reflectance, (c) a weak, sharp "spike" seen in some, but not all, samples, and (d) a flat reflectivity (of approximately 0.31 for good spectrally reflecting surfaces) for photon energies above the exciton energy.

The characteristic reflectance spectrum bears a resemblance to the well-known exciton reflectance in CdS.¹⁶ Both have strongly nonclassical spectral shapes and both exhibit the sharp spike. This similarity provides the first clue that polariton and spatial dispersion effects, whose importance have been adequately demonstrated in CdS, are important in GaAs.

A comparison of the data in Fig. 4 with the theoretical curves in Figs. 2 and 3 confirms that the polariton-spatial-dispersion theory does give a

good semiquantitative account of the data. The theoretical curve for $\theta \sim 90^\circ$ ($l \sim 290 \text{ \AA}$) gives the best agreement with the characteristic reflectance spectrum. In Fig. 4(b), the theoretical reflectance ($\theta = 90^\circ$, $\Gamma = 0$, nondegenerate bands) given by the dotted curve is compared with the reflectance data which exhibit the strongest minimum. The overall agreement strongly supports the conclusion that the spectrum represents the polariton reflectance for the $n=1$ free exciton. Further support is provided by transmission measurements⁴ on similar high-purity samples in which the sharp and exceedingly strong $n=1$ exciton absorption line is seen at an energy 0.1 meV below the energy for the reflectance spike. Both the strength of the observed reflectance structure and its energy coincidence with the strong absorption line rule out the possibility that it is an impurity-induced transition. Note also that no reflectance structure is seen at 1.5133 or 1.5141 eV, the energies at which impurity-induced luminescence and absorption⁴ are seen. Even though weakly bound excitons can have "giant" oscillator strengths,^{23,24} our samples are sufficiently pure that the reflectance is totally dominated by intrinsic free-exciton structure.

The polariton-spatial-dispersion theory can even account for the more unusual reflectance spectrum in Fig. 4(e). In this case a larger phase $\theta \sim 135^\circ$ ($l = 435 \text{ \AA}$) gives the best agreement with the data.

The reflectance spike can be very narrow. In some samples it is so sharp that we have observed a full width at half-maximum of 0.08 meV, which is limited by spectrometer resolution. In various samples we have observed the spike in the energy range 1.5150–1.5153 eV at 2 K. Since our photon energy calibration accuracy and day-to-day reproducibility are better than 0.1 meV, the observed variation is real and we obtain the energy $1.51515 \pm 0.00015 \text{ eV}$ for the spike. (In I we quoted the value 1.5151 eV.) The polariton-spatial-dispersion theory of Sec. IV predicts that the spike should occur at the longitudinal exciton energy E_L . This accurate experimental value for E_L is of considerable importance to our discussion and understanding of the polariton luminescence.

There are both experimental and theoretical reasons why the spike is seen in some samples but not in others which still exhibit the characteristic spectrum. As seen in Fig. 3, the spike is very sensitive to broadening. A small broadening of $\Gamma = 0.05 \text{ meV}$ completely suppresses the spike in the theoretical curve for $\theta = 90^\circ$. Experimentally we find that inhomogeneous strains introduced in mounting or in our stress experiments do suppress the spike. Another reason why the spike is sensitive to sample variations is that the phase $\theta \sim 90^\circ$ which accounts for the data is the limiting phase below which the spike does not occur in the theo-

retical curves. At $\theta=0^\circ$ the reflectance minimum occurs at the longitudinal exciton energy. At $\theta=90^\circ$ the minimum occurs at the transverse exciton energy and the spike emerges at the longitudinal energy. For $\theta=80^\circ$ the theoretical reflectance shape is almost identical with that at $\theta=90^\circ$ except that the spike does not occur. As the phase increases from $\theta=90^\circ$ to 180° the spike grows into the dominant feature of the spectrum and the $\theta=180^\circ$ spectrum is simply an inverted version of the $\theta=0^\circ$ curve (see Fig. 2). As a result, small variations (30 Å corresponds to a 10° change in phase) in the surface-barrier thickness, possibly caused by variations in surface parameters, can significantly affect the spike.

B. Longitudinal-Transverse Exciton Splitting

The longitudinal-transverse exciton energy difference is related to the polarizability β by the well-known relation²⁵

$$E_{LT} = E_L - E_T = \frac{2\pi\beta E_T}{\epsilon_0}. \quad (5.1)$$

The polarizability parameter β can be determined from the measured (or calculated) absorption coefficient at the band gap. Neglecting the spatial dispersion for the moment, the dielectric constant at energy E for an isolated oscillator at E_0 is given by

$$\epsilon(E) = \epsilon_0 + \frac{4\pi\beta E_0^2}{E_0^2 - E^2 - iE\Gamma} = \epsilon_1 + i\epsilon_2. \quad (5.2)$$

The integrated strength of $\epsilon_2(E)$ over the line is $2\pi^2\beta E_0$. If we equate this strength to the integrated $n=1$ exciton strength and assume that the exciton is hydrogenic, we obtain the relation

$$4\pi\beta = 4\hbar c \epsilon_0^{1/2} R_0^* \alpha(E_g) / \pi E_g^2, \quad (5.3)$$

where R_0^* is the exciton binding energy, and $\alpha(E_g)$ is the absorption coefficient at the band-gap energy E_g . From Sturge's experimental value³ $\alpha(E_g) = 0.95 \times 10^4 \text{ cm}^{-1}$, we obtain $4\pi\beta = 1.6 \times 10^{-3}$. This is the value used in Table II. Sturge's value for $\alpha(E_g)$ agrees quite well with the calculated value ($1.03 \times 10^4 \text{ cm}^{-1}$) obtained with Lawaetz's parameter²¹ $E_p = 25.7 \text{ eV}$ for the oscillator strength. For the parameters in Table II, Eq. (5.1) gives a value $E_{LT} = 0.1 \text{ meV}$ for the theoretical longitudinal-transverse splitting of the $n=1$ exciton.

The longitudinal exciton energy is defined as the energy of the interacting exciton and photon (i. e., polariton) at $\vec{K}=0$. (The transverse upper polariton branch must be degenerate with the longitudinal exciton at $\vec{K}=0$.) The sharp reflectance spike at $1.51515 \pm 0.00015 \text{ eV}$ occurs at the longitudinal exciton energy E_L . On the other hand, the transverse exciton energy is defined as the energy of the $\vec{K}=0$ exciton in the limit of zero exciton-photon interaction ($\beta \rightarrow 0$). For optical phonons with no

dispersion, the coupled phonon-photon states approach the transverse phonon energy for large K . In the present case for the exciton which includes spatial dispersion, the transverse exciton energy has no special significance for the polariton dispersion curves. Thus it is not surprising that E_T is more difficult to determine from experimental data. From Figs. 2 and 3 we see that the transverse exciton falls near the minimum of the reflectance curves for $\theta \sim 90^\circ$. The energy splitting between the spike and the reflectance minimum in the theoretical curves is 0.1 meV , in agreement with Eq. (5.1). Note that the coincidence of E_T with the reflectance minimum is not a general result, but rather depends upon the parameters in the theory. For the case of CdS, for example, the transverse exciton energy falls near the low-energy maximum of the reflectance spectrum.¹⁶

In the reflectance data, the minimum-to-spike energy difference is $0.25 \pm 0.05 \text{ meV}$. This is more than a factor of 2 larger than the theoretical value. We do not have an explanation for this difference beyond the point discussed below that the theory has numerous simplifying assumptions and that the surface barrier region, which has a strong effect upon the spectrum, is only partially understood. At present it appears reasonable to conclude that the actual longitudinal-transverse exciton splitting falls within the range $0.1\text{--}0.25 \text{ meV}$ set by our theoretical and experimental values.

C. Nature of the Surface Boundary Layer

We have emphasized that there is a characteristic experimental reflectance spectrum which is well accounted for by the polariton-spatial-dispersion theory. In general this is true, but there remain some specific points which deserve further discussion: (1) The data in Fig. 4 [except curve (e)] have a positive slope at energies below the reflectance minimum in contrast to the theoretical curves for $\theta=90^\circ$, which have a negative slope. The theoretical reflectance has a positive slope in this region for $\theta \sim 0^\circ$ (see Fig. 2) but then the spike does not occur and the overall agreement with experiment is worse. (2) The experimental longitudinal-transverse exciton splitting appears to be more than a factor of 2 larger than the theoretical value. (3) The amplitude of the reflectance minimum (relative to the background reflectance) is sample dependent even though the overall spectral shape does not change appreciably. For example, the amplitude in Fig. 4(c) is only 60% of that in Fig. 4(a). Since a small broadening is sufficient to destroy the sharp spike (see Fig. 3), it does not appear likely that the smaller amplitude in Fig. 4(c) is solely the result of broadening (unless Γ is strongly \vec{K} dependent, as discussed by Tait,²⁶ or the broadening is spatially inhomogeneous).

These specific points relate to a general question: What is the nature of the surface-barrier layer? The theory in Sec. IV as well as our data indicate that the surface barrier has a strong effect upon the reflectance. How well do we understand this surface barrier layer? Unfortunately, the answer is that our current understanding is rather limited.

Hopfield's model¹⁶ for the surface used in Sec. IV is quite simple. There is an impenetrable surface barrier with a sharp boundary a distance l from the flat crystal surface. Within the surface barrier the refractive index is taken to be real, spatially invariant, and frequency independent.

The actual surface conditions in our samples are almost certainly more complicated than this simple model. There are several mechanisms which tend to "repel" the excitons from the surface and thereby introduce a surface barrier. As the exciton approaches the surface (i. e., within a few exciton diameters), it experiences a repulsive induced-dipole force. The influence of the surface also tends to distort the exciton wave function. As the wave function is distorted, the exciton energy shifts and broadens such that the properties of the exciton are grossly changed. Thus, the free exciton of the bulk material in a sense does not "exist" in the surface layer. A third effect, similar to the preceding case, can arise from a surface space charge region. Other studies²⁷⁻²⁹ have shown that free surfaces of n -type GaAs tend to have depletion layers. The electric field in such depletion layers depends upon the impurity concentration and the surface states. In general this region can have fields adequate to badly broaden and ionize the exciton states as discussed by Blosssey.³⁰ This can create an absorptive surface barrier region in which the absorption could be as large as 10^4 cm^{-1} , the approximate band-edge absorption. Such an absorptive surface barrier might account for the sample dependence of the reflectance amplitude. This type of surface condition can be created in a reverse-biased Schottky diode with a semitransparent metal electrode. Such results have been reported recently by Evangelisti *et al.*¹¹ and have also been seen in this laboratory.³¹

Our data provide evidence that the surface barrier in our samples at 2 K is not caused by a conventional surface depletion layer. The depletion-layer thickness varies as the square root of the net donor concentration and hence would vary considerably from sample to sample. A "typical" depletion-layer thickness is large compared with the surface barrier thickness ($l \sim 290 \text{ \AA}$) we have discussed. For example, for $N_D^+ - N_A^- = 10^{13} \text{ cm}^{-3}$, and a band bending of 0.8 V, the depletion depth is 11 \mu m . Such a thick barrier would give a large-phase θ [Eq. (4.4)], but (neglecting the absorption

in the layer) the phase is measured modulo 2π [Eq. (4.3)]. Thus small fractional changes in the surface depletion layer thickness would cause large effective changes in θ and we would expect the reflectance structure to be strongly sample dependent if this mechanism were the cause for the polariton surface barrier. We note again that most as-grown surfaces and all carefully prepared free surfaces exhibit the characteristic reflectance spectrum of Fig. 4. This indicates that the surface barrier thickness, or phase, is essentially sample independent. We conclude that the depletion layer does not determine the surface barrier thickness. In fact, we can carry the analysis further and conclude that the band bending must be small in these samples otherwise it would determine the surface barrier thickness. A possible explanation is suggested by the fact that our samples are always subjected to a weak optical beam during these experiments. If the hole lifetime is long, the accumulation of holes at the surface will tend to flatten the bands. Our recent studies of the reflectance as a function of total sample illumination and temperature support these conclusions.³²

The point of the discussion in this section is that the surface barrier in real crystals is probably quite complicated and is not thoroughly understood. If we knew the actual surface conditions, this would provide a guide to an improved theory and hopefully the relatively minor discrepancies between the present simple theory and experiment could be resolved. This remains an area where further work is needed. For the present, we have used the simple theory of Sec. IV, but recognize that the actual barrier may be quite different from the simple one with thickness $l = 290 \text{ \AA}$ ($\theta \sim 90^\circ$) obtained from our comparison with the reflectance data. In any case, it is worth noting that a barrier thickness of 290 \AA is a physically reasonable result. It is essentially equal to one exciton diameter (273 \AA).

VI. LUMINESCENCE RESULTS

A. Data

Figure 5 presents a typical luminescence spectrum for these high-purity samples. We are primarily concerned with the narrow spectral region near the free-exciton energy, the region enclosed in the dashed box. However, before concentrating our attention there, we briefly discuss the whole low-temperature luminescence spectrum. Clearly, the spectrum is dominated by extrinsic behavior since most of the luminescence falls at energies well below the $n=1$ free-exciton energy near 1.515 eV. We find that our n -type samples with 77 K mobilities greater than $100\,000 \text{ cm}^2/\text{V sec}$ generally have very similar spectra. Lower-purity samples

tend to have broader, more poorly-resolved, and more complicated spectra. The spectrum in Fig. 5 is similar to that reported by others for comparable high-purity material.^{33,34}

This spectral region of GaAs has received much attention and numerous conflicting interpretations of the spectra have been given. The following interpretation of the luminescence spectrum appears to be reasonably well supported by experimental results: (a) The strong, sharp line near 1.5141 eV is due to recombination of excitons bound to neutral donors.^{33,35} (b) The line at 1.5133 eV has been associated with excitons bound to ionized donors,³⁶ but recent results support the contention that it could also arise from free-hole-neutral-donor transitions⁴ (or alternatively, that the binding energy of the hole is so small that the distinction is unimportant). (c) The weaker lines near 1.5123 eV have been associated with excitons bound to neutral acceptors.³⁶⁻³⁹ In our *n*-type samples the relative strength of these lines is quite sample dependent. (d) The weak lines in the region 1.509-1.512 eV have been identified as two-electron transitions in which a donor is left in an excited state.^{33,37} Beyond these transitions seen in Fig. 5, a typical spectrum includes weak structure near 1.49 eV associated with donor-acceptor-pair recombination and free-electron-neutral-acceptor recombination,⁴⁰ and a further weak structure near 1.5175 eV (too weak to be seen on the scale in Fig. 5) associated with recombination from free and/or bound excitons.^{4,10,37}

The spectral region of main interest here is shown in the dashed box in Fig. 5 and is shown more clearly in Fig. 6. The arrows in Fig. 6

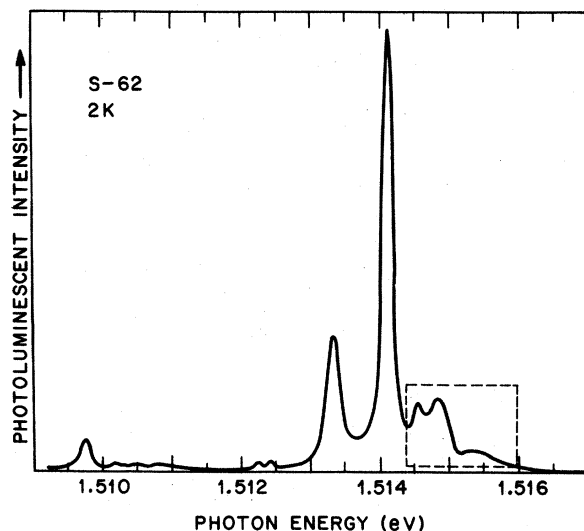


FIG. 5. A typical photoluminescence spectrum at 2 K for high-purity GaAs. A moderate He-Ne laser pump intensity of 1 mW/mm^2 was used.

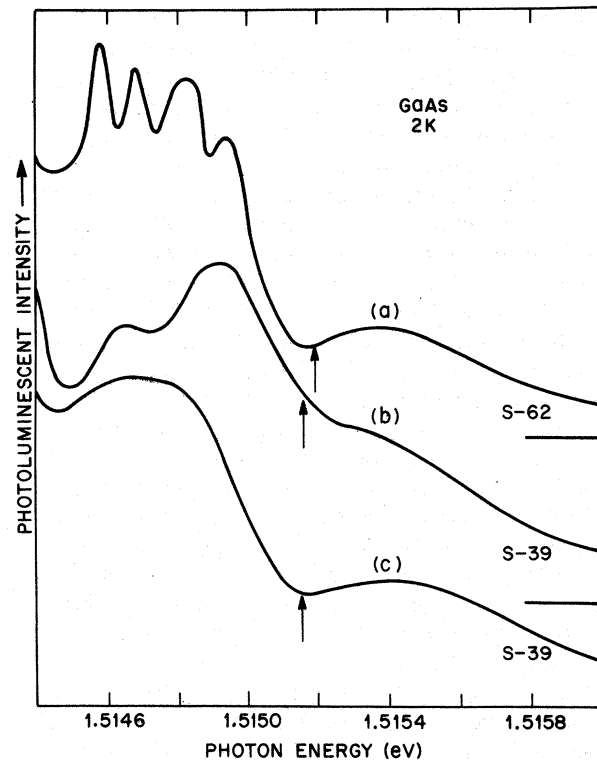


FIG. 6. Luminescence at 2 K in the narrow spectral region near the free exciton. The spectrometer resolution is approximately 0.08 meV. The laser pump intensity is approximately 1.0 mW/mm^2 for curves (a) and (c) and approximately 0.1 mW/mm^2 for curve (b). The luminescent intensity scale is arbitrary and different for the three curves to permit direct graphic comparison of the spectra.

indicate the longitudinal exciton energies for these samples as determined from the reflectance spectra. The luminescence occurring at slightly higher energies [with maxima near 1.5155 eV in curves (a) and (c)] has been identified in the past⁴¹ as the "free-exciton" luminescence. The remaining structure in Fig. 6 has generally been ascribed to bound excitons.³³ One of the main points of this paper is that these past interpretations of the spectra in Fig. 6 must be reconsidered in light of the new reflectance and absorption results.

Several points should be noted concerning the data in Fig. 6. The so-called "free-exciton" structure occurs at an energy above the longitudinal exciton energy determined from the reflectance. This structure is the only photoluminescence feature in the spectrum of Fig. 5 whose peak energy depends upon the laser pumping intensity even for low pump powers. This is demonstrated by spectral curves (b) and (c) for sample S-39. At intermediate pump intensities ($\sim 1 \text{ mW/mm}^2$ at the sample surface) as shown in (c) the peak occurs near 1.5155 eV. For higher pumping intensity the peak

broadens and moves to higher energy; however, the low-energy "onset" of the line still remains very near the longitudinal exciton energy (given by the arrow). Such behavior is also seen in the earlier work of Leite *et al.* (Fig. 1 of Ref. 42). For the low-pump-intensity data in Fig. 5(b) (~ 0.1 mW/mm²), the peak of the line appears to approach the longitudinal exciton energy asymptotically. Recently Bimberg and Schairer have reported quantitative results of energy shift versus pump power (Fig. 2 of Ref. 10). The important point which we wish to reemphasize is that, depending upon pump power, the peak of this structure occurs at or above the longitudinal exciton energy. Furthermore, the line is broad compared with other nearby transitions; the high-energy tail extends at least 1 meV above the longitudinal exciton energy. Generally speaking, this structure is not sample dependent. It was seen earlier in samples with 10 times the impurities in currently available samples. No significant sample dependence was observed for this structure for samples with $\mu_{77} \geq 10^5$ cm²/V sec.

The remaining structure in Fig. 6 shows a considerable sample dependence. In fact, the largest sample-to-sample variations for the whole spectral region of Fig. 5 are seen here. In some samples as many as four sharp resolved lines are seen [Fig. 6(a)]; in others, only two are seen [Fig. 6(b)]. Curves (b) and (c) also demonstrate that the relative strengths of these lines depend upon pump intensity. In curve (b) with low pump intensity, the lines sharpen and the higher-energy peak becomes dominant. We feel it is very significant that, in *all* high-purity samples we have studied (including the liquid phase epitaxial material), the highest-energy peak in this region (i. e., not including the "free-exciton" structure) coincides in energy with the reflectance minimum to an accuracy of better than 0.1 meV. In some cases the structure is only a shoulder. In some samples it is not clearly present for higher pump powers, but becomes much more evident at low pump intensity as seen in curves (b) and (c) for sample S-39.

B. Comparison with Reflectance

Figure 6 and the earlier results in I indicate that the so-called free-exciton luminescence occurs at an energy above that seen for the exciton in reflectance. This energy shift is of crucial importance to any interpretation of these spectra. Conceivably it could simply be the result of calibration errors, but as we have stressed, care has been taken to minimize such uncertainty. Another possibility, proposed by Bimberg and co-workers^{10,34} is that the exciton energy decreases with increasing laser excitation due to free-carrier screening.

Not only could this account for the observed pump-power dependence of the "free-exciton" luminescence discussed above, but it might also explain why the exciton appears to have different energies in reflectance and luminescence spectra. Reflectance spectra, particularly in a double-beam configuration such as ours, are generally taken under low illumination conditions, where such screening would be much less important.

In order to clarify this situation we have performed a series of experiments to compare directly the reflectance and luminescence spectra of a given area of a given sample for different laser pump intensities. The apparatus is discussed in Sec. III C and is illustrated in Fig. 1. A typical result is shown in Fig. 7. The photoluminescence was obtained with a He-Ne laser pump intensity of 1.6 mW/mm². The reflectance for this sample illuminated by this *same* laser beam and also a weaker probe lamp is shown as the solid curve. Finally, the reflectance with the laser off is given by the dashed curve. It is quite clear that the reflectance structure does not shift for this laser illumination even though the luminescence peak has shifted to 1.5155 eV, an energy well above the reflectance structure. Both reflectance spectra in Fig. 7 are of the characteristic form shown in Fig. 4.

From these experiments we conclude that the "free-exciton" luminescence peak does not provide a reliable measure of the true free-exciton energy. The combined facts that the exciton reflectance is essentially independent of optical-pumping intensity over a wide range of illumination and that the reflectance itself is comparatively well understood, both strongly argue that it is the reflectance, not the luminescence, which provides the more direct

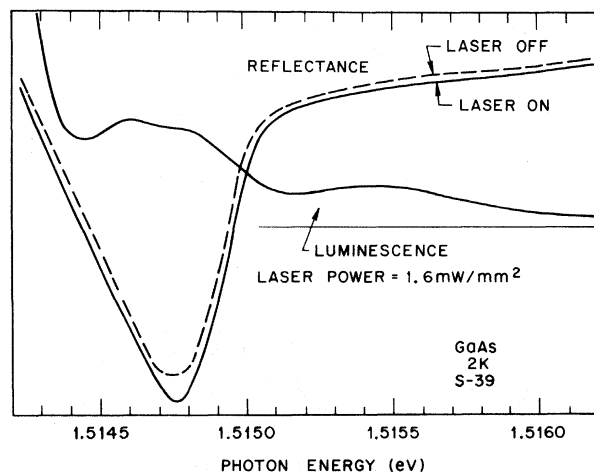


FIG. 7. A direct comparison of the luminescence and reflectance (laser on, solid curve; laser off, dashed curve) using the experimental configuration in Fig. 1.

and reliable measure of the exciton energy, and that a new interpretation of the luminescence must be considered. We further conclude that the energy shift of the exciton luminescence with pump intensity does not arise from free-carrier screening as proposed by Bimberg and co-workers.^{10,34} Even including a spatially varying electron concentration, it is difficult to envision a situation in which the excitons (or polaritons) important for luminescence are screened whereas those important for reflectance are not. Rather, it appears that we must seek a different explanation for this energy shift in the luminescence. Such an explanation is given in the next section.

C. Interpretation of Luminescence Results

The photoluminescence process is very complicated in real crystals. It is considerably more difficult to analyze than either reflectance or transmittance spectra. In the latter two cases we deal with weak optical illumination which leaves the sample in thermal equilibrium but which "probes" its dielectric function. The difficulties in the theory arise in determining a proper model for the dielectric function and in including realistic surface boundary conditions. For the case of luminescence these same problems exist, but there are numerous other difficulties. The sample is not in thermal equilibrium. Many of the bulk and surface scattering and trapping parameters which strongly affect the luminescence are generally not known. To our knowledge, there is no quantitative theory to describe the intrinsic luminescence in GaAs. Here we present a reasonable qualitative description of these experimental results. Hopefully our data will help to generate a renewed interest in the theory of intrinsic photoluminescence.

Since polariton and spatial-dispersion effects are both important for the reflectance spectrum, we naturally consider these effects in the luminescence as well. Figure 8(a) illustrates the calculated polariton E versus K for the $n=1$ exciton in GaAs using the appropriate parameters in Table II. For simplicity we have shown only the two optically active transverse branches which we refer to as the upper (UPB) and lower polariton branches (LPB) as shown in Fig. 8(a). The UPB is degenerate with the longitudinal exciton at $K=0$ and becomes essentially photonlike for energies a few millivolts above the transition energy. The LPB is photonlike for small K and excitonlike for large K . Note that even though the longitudinal-transverse splitting is only 0.1 meV, there is an energy range of approximately 2 meV over which excitonlike and photonlike states are strongly mixed.

The data firmly support the interpretation that the intrinsic luminescence is occurring from *both* the upper and lower polariton branches. In this

model, the peak near 1.5155 eV in Fig. 6 is associated with the UPB. This explains why it occurs at an energy above the longitudinal exciton energy and also accounts for the fact that its "onset" appears at the longitudinal energy. In this model the energy of the peak of this structure is determined by the various transition probabilities (including thermal factors) into and out of the UPB and bears no unique relation to the exciton transition energy. The fact that the peak tends to approach the longitudinal exciton energy for low pumping intensity is quite consistent with this in-

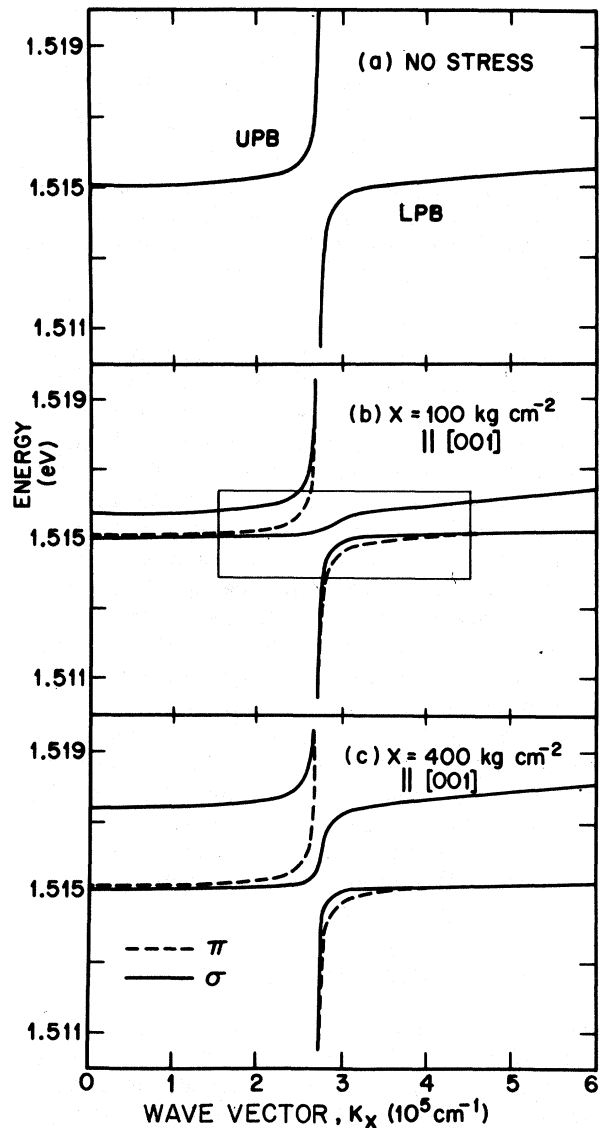


FIG. 8. Calculated polariton dispersion curves for the $n=1$ exciton of GaAs for (a) no stress and (b), (c) for stress parallel to the [001] axis. π and σ refer to linear polarization of the photon electric field parallel and perpendicular to the stress, respectively.

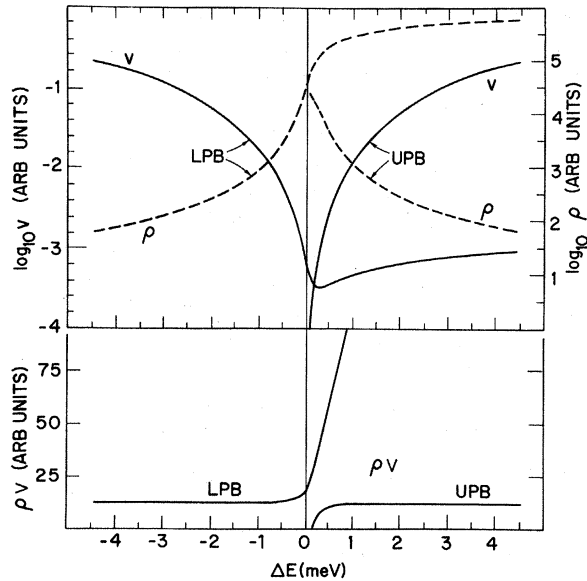


FIG. 9. Calculated density of states ρ (dashed curve), group velocity v (solid curve) and product ρv for the LPB and UPB polaritons in GaAs. The energy zero corresponds to the transverse exciton energy.

terpretation. Similarly, we associate the luminescence which occurs near the energy of the reflectance minimum (and transverse exciton energy) with the conventional lower polariton branch luminescence. This is consistent with the theoretical arguments that the LPB luminescence should occur near the "knee" of the dispersion curve.⁴³ In our interpretation, there are two luminescence peaks ascribed to free-exciton decay. The structure previously assigned as "free-exciton" luminescence arises from the UPB and one of the lines previously thought to be due to bound excitons is interpreted as the usual LPB emission.

The work of Tait and Weicher^{44,45} provides at least a qualitative guide to determine the feasibility of our interpretation and to consider other possible models. Assuming quasithermal equilibrium (along with other simplifying assumptions spelled out in Ref. 44) the photon emission rate per unit area at energy E is given by

$$\omega(E) = \sum_f \frac{D\alpha_f(E)J_f(E)T_f(E)}{D\alpha_f(E)+1}, \quad (6.1)$$

where D is the effective diffusion length, α_f , J_f , T_f are the absorption coefficient, current density, and surface transmissivity for the polariton branch f and the sum over f includes both UPB and LPB contributions. For the spectral region near the exciton energy where $D\alpha_f \gg 1$, Eq. (6.1) simplifies to

$$\omega(E) = \sum_f J_f(E)T_f(E) \sim \sum_f \rho_f(E)v_f(E)N_f(E)T_f(E), \quad (6.2)$$

where ρ_f , v_f , and N_f are, respectively, the density of states, group velocity, and population per mode at energy E for the branch f . We have calculated ρ_f and v_f for the polariton model of Sec. IV A. The results are shown in Fig. 9. Although both ρ_f and v_f vary considerably (note the log scales), the product $\rho_f v_f$ is not a strong function of energy. Furthermore, the value of ρv for the LPB at or below the exciton energy is essentially equal to that for the UPB in the region just above the longitudinal exciton energy. Since quasithermal equilibrium was assumed, $N_f(E)$ simply introduces the factor $e^{-E/kT}$, where T is an "effective" temperature for the pumped crystal. If we take the high-energy tail of the UPB luminescence as a measure of $N(E)$, we estimate an effective temperature of approximately 5 K for typical pumping intensities and for the sample immersed in liquid helium at 2 K. The transmissivity factor $T_f(E)$ for the lower branch is $1 - R(E)$ (~ 0.7) below the transverse exciton energy (i. e., below the knee of the dispersion curve) and rapidly becomes very small above this energy because the LPB becomes predominantly excitonlike. In the absence of broadening, $T_f(E)$ is zero for the UPB below the longitudinal exciton energy (the propagation vector is pure imaginary) and becomes essentially equal to $1 - R(E)$ above the longitudinal energy. If we estimate⁴⁶ $D \sim 10 \mu\text{m}$ then the approximation $D\alpha_f \gg 1$ is only valid for a range of approximately ± 0.5 meV about the exciton energy. Outside this range Eq. (6.1) must be used and $\omega(E)$ becomes proportional to $\alpha_f(E)$.

With this simple model we obtain a reasonably good qualitative account of the data. The luminescence peak near the transverse exciton energy arises from the LPB. Its shape is primarily determined by the increasing absorption coefficient at low energy and the decreasing transmissivity above the "knee" in the LPB dispersion curve [also $N(E)$ will decrease below the knee because the quasiequilibrium approximation will break down in this region]. The luminescence peak above the longitudinal exciton energy arises from the UPB. Its shape is determined by increasing transmission and ρv (see Fig. 9) factors at low energy and by decreasing $N(E)$ and $\alpha_f(E)$ at high energy.

In considering other alternative models, the key point is to explain the luminescence which extends well above the longitudinal exciton energy. If we exclude the UPB, this luminescence would have to arise from the LPB or the longitudinal exciton branch (with K values in the range $3 \times 10^5 \lesssim K \lesssim 10^6 \text{ cm}^{-1}$). Although the product ρv increases and thus tends to favor LPB (and longitudinal exciton) transmissions in this spectral range (see Fig. 9), both $T_f(E)$ and $\alpha_f(E)$ [in Eq. (6.1)] strongly discriminate against such a process. Furthermore, for flat smooth surfaces the longitudinal exciton does not

couple to the photons. We might argue that such coupling could be introduced by surface roughness, but then it would be difficult to explain why the luminescence does not appear to change appreciably for samples with very different surface topography.

Gross and co-workers⁴⁷ have recently studied the polariton luminescence in CdS. They observed a doublet structure with both peaks below the longitudinal exciton energy and concluded that in this case both must be due to lower branch (LPB) luminescence. They suggested that the same interpretation should apply to GaAs; however, their arguments do not apply since the upper peak in GaAs occurs well above the longitudinal exciton energy.

To summarize, we observed two luminescence features associated with the free exciton, and have considered the three cases in which the two peaks arise from (1) LPB plus UPB, (2) only LPB, and (3) LPB plus the longitudinal exciton branch. Of these, we feel that the longitudinal exciton case can be ruled out. The LPB case is possible, but the simple theory discussed above tends to rule against it in favor of the LPB plus UPB interpretation. All of our data are consistent with the LPB plus UPB interpretation. Even the anticrossing behavior seen for uniaxial stress (Sec. VII C) lends support to this conclusion.

It is worth noting that this is a rather new and unique result. The only previous case in which UPB luminescence has been seen is in CdS for a very special geometry of extraordinary light waves weakly coupled to mixed transverse-longitudinal exciton modes.⁴⁸ In GaAs we see clearly resolved UPB luminescence for transverse excitons and can study its behavior for various external perturbations (e.g., stress).

VII. STRESS RESULTS

A. Theory

In this section we briefly discuss the theoretical background necessary to interpret our stress results. It is convenient to begin with a group-theoretical discussion of the exciton states in the unstrained crystal and then actually diagonalize the Hamiltonian for the strained crystal, bearing in mind that the wave functions thus obtained must conform to the general restraints imposed by group theory.

The unstrained crystal symmetry is T_d . We use the symmetry notation of Koster *et al.*⁴⁹ and note that since the $n=1$ exciton envelope function of interest is an s function, the exciton symmetry is simply given by the usual direct product representations of the electrons and holes. (We also assume that the exciton binding energy is independent

of stress.) Including spin degeneracy, there are six p -like Γ_5 upper-valence-band states and two s -like Γ_1 conduction-band states for a total of 12 exciton substates. In our case for GaAs the 340-meV spin-orbit splitting of the valence band is large compared with either the strain or exciton-exchange energies. Consequently, the 12 states are split into two groups: One group of eight states for the upper-valence bands ($j = \frac{3}{2}$) of interest here, and four states for the split-off valence bands ($j = \frac{1}{2}$) which have little effect upon our results. In the absence of strain, these eight exciton states transform as Γ_3 , Γ_4 , and Γ_5 . Of these, only the threefold degenerate Γ_5 state couples with the light.

We could continue with this approach to determine the symmetry properties of the stressed crystal; however, it is convenient at this point to diagonalize the Hamiltonian of the stressed crystal to obtain the eigenvalues and eigenfunctions for the various levels of stress and for different exchange parameters. We follow the approach of Langer *et al.*⁵⁰ who give in their Table I the 12×12 matrix including a general strain energy, exciton exchange, and the spin-orbit interaction for a zinc-blende material. We consider the case of an [001] uniaxial compressive stress (z axis) with the light propagating perpendicular to the stress (call this the x axis). For an [001] stress the 12×12 matrix reduces to two 6×6 matrices. One matrix couples to π -polarized light (\vec{E} parallel to the stress axis); the other one couples to σ -polarized light (\vec{E} perpendicular to stress, i.e., $\vec{E} \parallel y$ axis). Clearly there can be no mixing of the states or transfer of intensity between the π and σ spectra in this case. Earlier work⁵¹ indicates that the stress behavior of these bands is nearly isotropic (i.e., nearly the same for any direction of uniaxial stress). Consequently our calculations for an [001] stress also apply for our [110] stress experiments.

We have diagonalized these two 6×6 matrices with a digital computer to obtain the energies and optical transition strengths for each of the 12 exciton substates as a function of the various parameters. Figure 10 illustrates the energy-versus-stress results for parameters which should give a reasonable account of the data. We continue to use the T_d symmetry notation of the unstrained crystal to illustrate how the eigenstates evolve as a function of stress. In this notation, $\Gamma_3(1)$ and $\Gamma_3(2)$ are the two substates of Γ_3 , $\Gamma_5(z)$ is the z -like partner function of an x, y, z basis of Γ_5 , and $\Gamma_4(3)$ is the S_z -like basis state of Γ_4 . The stress mixes the x, y - and S_x, S_y -like basis states of Γ_5 and Γ_4 , respectively. The four resulting states, denoted by x_1, y_1 and x_2, y_2 , couple to light of σ polarization and the $\Gamma_5(z)$ state couples to π polarized light. We note that five of the eight sub-

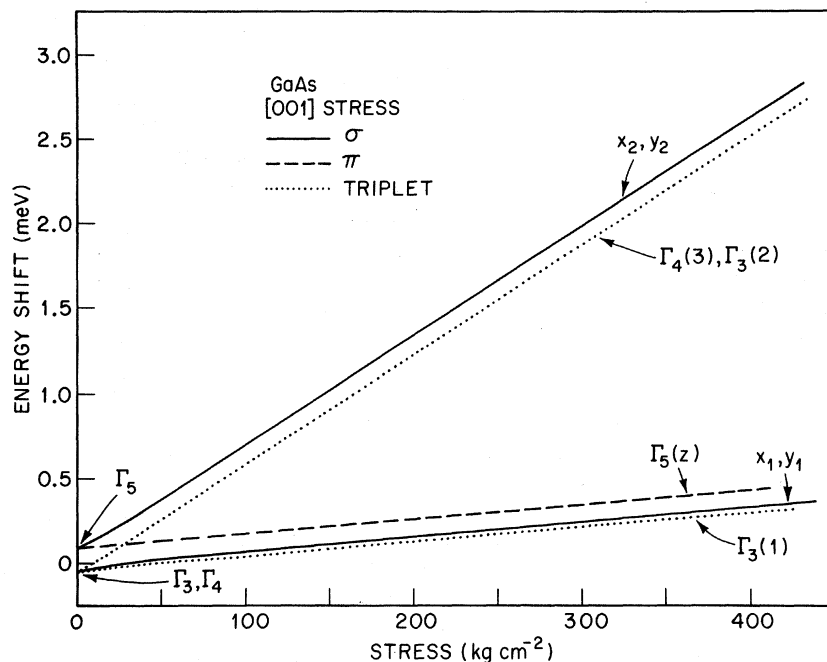


FIG. 10. Calculated exciton energies as a function of [001] uniaxial stress based upon the stress-exchange Hamiltonian in Ref. 50 with the following parameters: $j = -0.1$ meV, $\Delta = -113$ meV (spin orbit sp splitting $= 3\Delta$), $C_1 = a - 2b = -4.7$ eV, and $C_2 = 3b = -6.0$ eV. For the conventions adopted in Ref. 50, Δ must be negative to obtain the proper ordering of the spin-orbit-split exciton states. The values $a = -8.7$ eV and $b = -2.0$ eV were obtained from Ref. 51. The abscissa uses positive values to denote compressive stress. (In the actual matrix calculation we used the usual convention $X < 0$ for compressive stress.)

states couple to light in the stressed crystal while only three couple in the unstressed case.

The exciton exchange has been included as a Heisenberg-like term in the Hamiltonian

$$H_{\text{ex}} = \frac{1}{2} j \sigma_h \sigma_c, \quad (7.1)$$

where j is the exchange constant and σ_h and σ_c operate on valence hole and conduction electron states, respectively. From physical arguments we expect a negative j ; that is, the energy of the triplet states Γ_3 and Γ_4 should be lower than the singlet state Γ_5 for zero stress. In Fig. 10 we have taken the value $j = -0.1$ meV since this is an upper limit to the exchange value determined by the reflectance data presented in the next section.

It is important to note a point that appears not to be generally appreciated: The singlet-triplet splitting at zero stress is $-4j/3$ if the spin-orbit splitting is large compared with j . It is well known that this single-triplet splitting is $-2j$ for zero spin-orbit splitting. For stress such that the energy separation between states x_1 and x_2 is large compared with j (but yet small compared with the spin-orbit splitting), we obtain the important result that the energy difference between the π polarized state [$\Gamma_5(z)$] and the lower σ polarized states (x_1, y_1) asymptotically approaches the value $-j$ (i. e., splitting $\geq |j|$). In Fig. 10 this splitting decreases from $\frac{4}{3}j$ to j at stress levels below 50 kg cm^{-2} . Therefore, the energy shift, if any, between the π and lower σ reflectance structure is a direct measure of j .

For $j = 0$, the σ -polarized states x_1, y_1 are de-

generate with the π -polarized state $\Gamma_5(z)$, and group theory determines the ratio of the intensities of the three transitions $\Gamma_5(z)(\pi)$, $y_1(\sigma)$, and $y_2(\sigma)$ to be 4 : 1 : 3. (For stress parallel to z and k parallel to x , σ polarization couples only to states y_1 and y_2 .) Even with exchange included as in Fig. 10, the total π and σ intensities remain unchanged; however, for low stress levels (stress $\lesssim 200$ kg cm^{-2}), the ratio of the y_2 to y_1 intensities is greater than 3. For larger values of stress the intensities approach the same 4 : 1 : 3 ratio.

B. Reflectance Data and Determination of Exchange Energy

Figure 11 presents reflectance data for [110] stress. The observed splitting and polarization behavior are in good agreement with the calculated results in Fig. 10. The energy shifts with stress agree within combined experimental errors ($\pm 15\%$) with those obtained by Pollak and Cardona⁵¹ by piezoelectroreflectance. These results provide further support for the identification of this reflectance structure with the $n = 1$ free exciton.

Langer and co-workers⁵⁰ have demonstrated in their work on II-VI compounds that piezoreflectance data provide a direct measure of the exchange energy discussed in the previous section. Figure 12 presents reflectance spectra for a uniaxial stress of 330 kg cm^{-2} along the [001] axis. The two polarized spectra were taken consecutively without altering the applied stress. There is only a slight hint of a displacement of the lower-energy σ spectrum with respect to the π spectrum. We have carefully measured this relative shift of π and σ

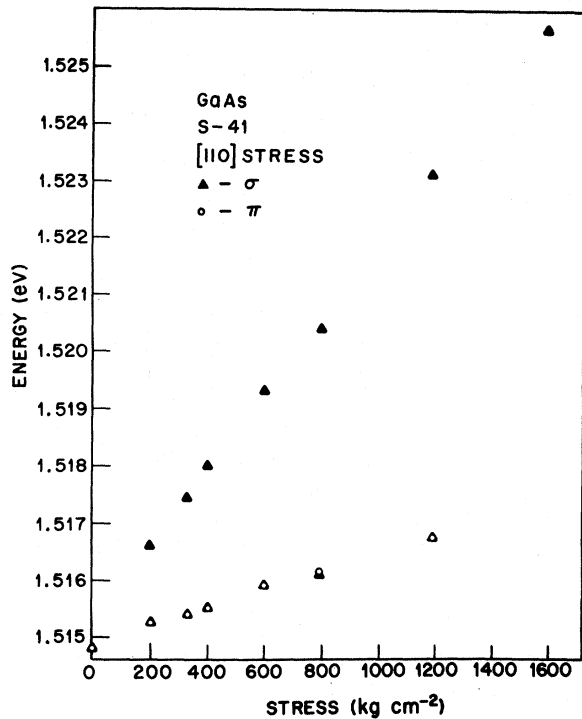


FIG. 11. Experimental exciton energies as a function of [110] compressive uniaxial stress. The energy was taken as the minimum of the reflectance curve. The lower energy σ - and π -line energies are essentially degenerate on this energy scale.

spectra for both [001] and [110] uniaxial stress in the range 100–1600 kg cm⁻² and conclude that the shift must be less than 0.1 meV. This determines an unambiguous value $j = -0.05 \pm 0.05$ meV, in direct contrast to the value 0.37 meV obtained previously by Gileo, Bailey, and Hill⁵² from stressed luminescence studies. We have already pointed out in Sec. VI that the luminescence data require considerable interpretation and do not necessarily give good values for the exciton energy. For this

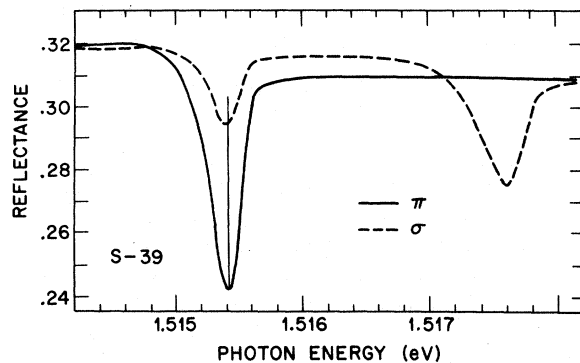


FIG. 12. Polarized reflectance spectra for a [001] compressive stress of $X=330$ kg cm⁻².

and other reasons discussed in the next section we conclude that the previous value of 0.37 meV is incorrect.

The new, smaller value for the exchange has been used by Sell⁴ to interpret exciton absorption results and obtain the value 4.2 ± 0.2 meV for the exciton binding energy. This value agrees well with the value 4.1 meV calculated from the exciton theory of Baldereschi and Lipari.²⁰

C. Luminescence

Figure 13 presents the same stress results given earlier in I. The luminescence behavior is more complicated than the reflectance because we have both the LPB and UPB peaks. The important result is that both the UPB and LPB structures exhibit the same splitting and polarization behavior as predicted by theory (Fig. 10) and seen for the reflectance (Fig. 11). We find that all of the structure of Fig. 5 from the 1.5133-eV line through the UPB luminescence exhibits nearly this same splitting pattern determined by the free electron and hole deformation potential constants. (This is contrary to our earlier statement in I that the 1.5141-eV line appeared to have a different splitting behavior.)

Our piezoluminescence results in Fig. 13 for the UPB structure are nearly the same as the work of Gileo, Bailey, and Hill⁵² (their Fig. 2). Their X_{1a} , X_{1b} , and X_2 transitions all correspond to the transitions labeled UPB in Fig. 13. The differences are that we see an anticrossing in the UPB π spectrum at low stress (discussed below) and that we have studied the LPB structure which has a higher-energy stress component in the region of the UPB

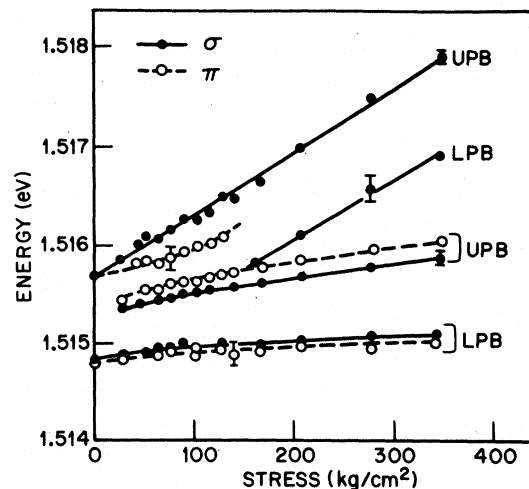


FIG. 13. Stress results at 8 K for a [001] compressive uniaxial stress. The solid and open circles are the peaks of the luminescence structure for σ (\vec{E} perpendicular to stress) and π (\vec{E} parallel to stress), respectively.

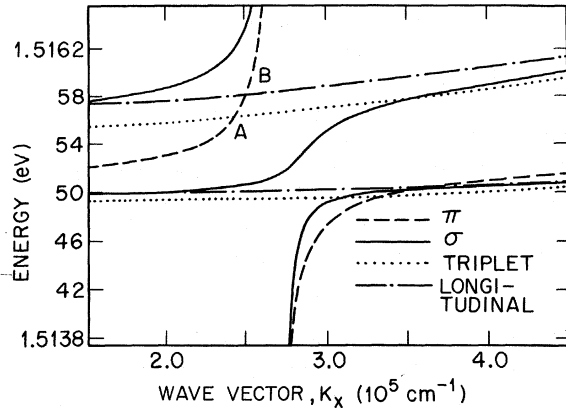


FIG. 14. Calculated polariton dispersion curves for $X=100 \text{ kg cm}^{-2}$ along [001] as in Fig. 8(b) but including all eight exciton states.

luminescence not reported by Gilleo *et al.* The main differences are in the interpretation of the data. As discussed above, we interpret their "free-exciton" data (Figs. 1 and 2 of Ref. 52) as UPB luminescence. We also disagree with their contention that these data determine an exchange splitting of 0.37 meV for the following reasons: (a) It is not supported by the reflectance data which should provide a direct and reliable determination of the exchange. (b) In general, our results indicate that the peaks of the polariton luminescence structure, particularly the UPB peak, do not provide an accurate measure of the exciton energy. (c) Even if one assumes for the moment that the exchange interaction causes the observed energy difference $[X_{1a}(\pi) - X_{1b}(\sigma)]$, their data do not firmly support the value 0.37 meV, obtained by extrapolating the observed splitting to zero stress (therefore, $j = -\frac{3}{4} \times 0.37 = -0.28 \text{ meV}$). Their observed splitting of 0.12 meV at high stress should provide a more reliable measure of the exchange energy; this value ($j = -0.12 \text{ meV}$) is close to our result obtained from the reflectance data.

In Fig. 13, for low stress, the π -polarized UPB structure consists of two peaks which suggest an anticrossing behavior. This anticrossing has the following characteristics: (a) It is seen in π but not in σ polarization. This rules out the possibility that it is caused by an interaction with an optically active σ polarized state and suggests that an optically forbidden exciton state is involved. (b) It occurs for both [001] and [110] stress. (c) As the pump intensity is increased and the peak of the UPB luminescence moves to higher energy, the anticrossing also moves to higher stress levels.

An anticrossing occurs when two levels tend to cross, but instead are mixed and repelled. It is well known that for an interaction matrix element V , the minimum separation of the anticrossing

states is $2|V|$. To understand this anticrossing we must consider the stress dependence of the eight exciton states (see Fig. 10) as a function of \vec{K} including the exciton-photon interaction. Figure 8 illustrates the calculated polariton dispersion curves for the optically active exciton states for two values of stress. It is clear that the π -polarized UPB does not tend to intersect with the σ -polarized UPB. If it did, the anticrossing would also occur in σ polarization, contrary to our data. In Fig. 14 we look more closely at the region within the box in Fig. 8(b) (for $X=100 \text{ kg cm}^{-2}$) and include all eight exciton states. At the points marked A and B the π -polarized UPB crosses the triplet states $[\Gamma_4(3) \text{ and } \Gamma_3(2)]$ and the longitudinal exciton, respectively. The states do not interact at points A and B for the Hamiltonian used to this point; however, such interactions could possibly arise when valence-band anisotropy and linear- K terms are included. We will not go into the details here, but it is not difficult to show that the linear- K term, including the stress-induced term of Sakoda and Onodera,⁵³ is too small to account for the observed anticrossing. In fact, for [001] stress and K along [010], the linear- K coupling terms are zero at points A and B. The valence-band anisotropy does introduce a coupling at point A between the π -polarized UPB $[\Gamma_5(z)]$ and the triplet states $\Gamma_3(2)$ for [001] stress and $\Gamma_4(3)$ for [110] stress (assuming that K is perpendicular to the stress in each case). The estimated strength of this anisotropy interaction term (for Lawaetz's valence-band parameters²¹) is only approximately a factor of 2 smaller than the observed anticrossing splitting and generally predicts a behavior consistent with our data.

It is significant that the details of the data, such as this anticrossing, are accounted for in our UPB interpretation of the exciton luminescence. If instead, we identify this luminescence at 1.5155 eV with the LPB, this explanation for the anticrossing does not apply and we do not have an alternative explanation. We feel that the observed anticrossing provides strong indirect support for the UPB interpretation of the luminescence.

VIII. TEMPERATURE DEPENDENCE OF THE LUMINESCENCE

All of the results presented so far (except the luminescence-stress data of Sec. IID) have been for samples immersed in pumped liquid helium at 2 K. In addition, both reflectance and luminescence spectra have been studied as a function of temperature. The reflectance results are presented elsewhere.³² Except for the fact that they indicate that the low-temperature band bending is small, these results are not particularly relevant to this paper and will not be discussed here. The temperature

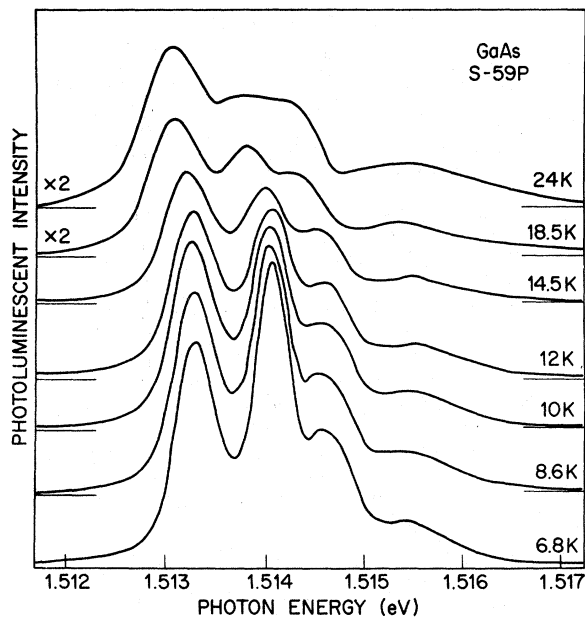


FIG. 15. Temperature dependence of the luminescence spectrum. The sample was cooled by flowing helium gas.

dependence of the luminescence, however, does provide additional evidence for our interpretation of the luminescence spectrum. These results are presented in Fig. 15. The spectrum at 6.8 K is somewhat broader than that in Fig. 5 but otherwise is essentially the same as the 2-K spectrum. As the temperature is raised to 24 K all of the structure, except the highest-energy peak, shifts slightly to lower energy due to the temperature dependence of the band gap (seen also in reflectance). Up to 24 K the various spectral features retain their identities, but at slightly higher temperatures only a weak and rather broad band is seen.

The peak near 1.5141 eV has the strongest temperature dependence. This behavior is consistent with its identification as decay of an exciton bound to a neutral donor. The binding energy of approximately 0.8 meV for this center corresponds to a temperature of approximately 10 K. As the temperature is raised the (D^0, X) complex thermally dissociates into a neutral donor D^0 and a free exciton, and the 1.5141-eV line loses its intensity. The fact that the other features do not have such a strong temperature dependence argues that these features do not involve weakly bound exciton complexes.

These data are consistent with our interpretation of the LPB luminescence near 1.5148 eV. The results are totally inconsistent with the previous interpretation of this structure as bound-exciton luminescence. If this were the case, the temperature dependence of this luminescence should be

even stronger than that of the 1.5141-eV line. Clearly this is not the case.

The temperature dependence of the highest-energy luminescence supports our identification of it as UPB emission. For increasing temperature the peak shifts even further above the longitudinal exciton energy, but the low-energy "onset" remains at the longitudinal energy. At 24 K this luminescence extends more than 2 meV above the exciton energy seen in the reflectance data.

IX. EXCITED EXCITON STATES

To this point, we have concentrated upon the $n = 1$ free exciton. What about higher free-exciton states? The $n = 1, 2$ free-exciton transitions are well resolved in the low-temperature absorption data for similar high-purity samples. These results⁴ determine that the $n = 2, 3$ and band-gap energies at 2 K are 1.5183, 1.5189, and 1.5192 eV, respectively, and that the $n = 1$ exciton binding energy is 4.2 meV. Bimberg and Schairer¹⁰ have reported two weak luminescence features at 1.5176 and 1.5182 eV which they claim are to be associated with the $n = 2, 3$ free-exciton states; however, their supporting evidence is not strong. The absorption results⁴ leave little doubt that their interpretation of these luminescence data is incorrect. Their lower energy luminescence line at 1.5176 eV appears to be impurity related; the line at 1.5182 eV may be $n = 2$ free-exciton luminescence.

The simple hydrogenic approximation for the free exciton is reasonably accurate in GaAs. This simple theory gives a good account of the observed strength of the $n = 1$ reflectance structure (used in Sec. VB to obtain β) and the $n = 2, 3$, and band-gap absorption data. The theory also predicts that the amplitude of the reflectance structure for the $n = 2$ free-exciton transition should be well above the peak-to-peak noise of 0.0005 in the reflectance data obtained with the double-beam reflectance apparatus. Such structure is conspicuously absent from the data of Fig. 4. Weak structure is seen near 1.5177 eV in Fig. 4(c); however, we do not associate that with the $n = 2$ exciton for the following reasons: (a) It occurs only in the relatively few samples which have the unusual $n = 1$ reflectance shape of Fig. 4(e). When the samples are etched and the $n = 1$ reflectance returns to the characteristic shape, this weak structure is no longer seen. (b) Its energy does not agree with the 1.5183-eV value obtained for the $n = 2$ exciton state in the absorption data.

It is possible that weak surface electric fields (not included in the theoretical estimates above) might quench the $n = 2$ exciton. The $n = 2$ exciton has such a large radius (~ 1150 Å) that a field on the order of 160 V/cm is sufficient to ionize it and

hence broaden it to the point that it would not be seen. Since the ionization field for an $n=1$ exciton is 2.6×10^3 V/cm, it is possible to have a situation in which the surface field has little effect upon the $n=1$ exciton but yet strongly perturbs the $n=2$ exciton state.

ACKNOWLEDGMENTS

The authors thank John Hopfield and Evan Kane for several helpful discussions, and acknowledge the capable assistance of K. W. Wecht and K. F. Rodgers with the experiments.

*Present address: Corporate Research and Development Laboratory, Martin Marietta Corp., Baltimore, Md. 21227.

[†]On leave of absence at Australian National University, Canberra, Australia.

¹D. D. Sell, R. Dingle, S. E. Stokowski, and J. V. DiLorenzo, Phys. Rev. Lett. **27**, 1644 (1971), referred to as I in text.

²E. W. Williams and H. B. Bebb, in *Semiconductors and Semimetals*, edited by R. K. Willardson and A. C. Beer (Academic, New York, 1972), Vol. 8, p. 321.

³M. D. Sturge, Phys. Rev. **127**, 768 (1962).

⁴D. D. Sell, Phys. Rev. B **6**, 3750 (1972).

⁵D. E. Hill, Solid State Commun., **11**, 1187 (1972).

⁶J. L. Shay and R. E. Nahory, Solid State Commun. **7**, 945 (1969).

⁷D. D. Sell, Appl. Opt. **9**, 1926 (1970).

⁸B. N. Taylor, W. H. Parker, and D. N. Langenberg, Rev. Mod. Phys. **41**, 375 (1969).

⁹See U. S. Natl. Bur. Std. Monograph **3**, Vol. I (1960).

¹⁰D. Bimberg and W. Schairer, Phys. Rev. Lett. **28**, 442 (1972).

¹¹F. Evangelisti, A. Frova, and J. U. Fischbach, Phys. Rev. Lett. **29**, 1001 (1972).

¹²D. D. Sell and E. O. Kane, Phys. Rev. **185**, 1103 (1969).

¹³J. V. DiLorenzo and A. E. Machala, J. Electrochem. Soc. **118**, 1516 (1971); and J. V. DiLorenzo (unpublished).

¹⁴L. J. van der Pauw, Philips Res. Rep. **13**, 1 (1958).

¹⁵D. L. Rode and S. Knight, Phys. Rev. B **3**, 2534 (1971); D. L. Rode (private communication).

¹⁶J. J. Hopfield and D. G. Thomas, Phys. Rev. **132**, 563 (1963), referred to as HT in text.

¹⁷J. J. Hopfield, J. Phys. Soc. Jap. **21**, 77 (1966); Phys. Rev. **112**, 1555 (1958).

¹⁸Recently J. J. Sein [J. Opt. Soc. Am. **62**, 1037 (1972)] has discussed a different additional boundary condition which replaces our Eq. (4.5) with a different effective index $n^\dagger = n_1 + n_2 - qc\omega^{-1}$, but which retains the surface boundary layer of HT. We have calculated the reflectance with Sein's expression for n^\dagger and find that it does not agree with our experiment as well as the HT theory does.

¹⁹E. O. Kane (unpublished).

²⁰A. Baldereschi and N. O. Lipari, Phys. Rev. B **3**, 439 (1971).

²¹P. Lawaetz, Phys. Rev. B **4**, 3460 (1971).

²²G. D. Mahan and J. J. Hopfield, Phys. Rev. **135**, A428 (1964).

²³E. I. Rashba and G. E. Gurgenishvili, Fiz. Tverd. Tela **4**, 1029 (1962) [Sov. Phys.-Solid State **4**, 759 (1962)].

²⁴C. H. Henry and K. Nassau, Phys. Rev. B **1**, 1628 (1970).

²⁵J. J. Hopfield and D. G. Thomas, J. Phys. Chem. Solids **12**, 276 (1960).

²⁶W. C. Tait, Phys. Rev. B **5**, 648 (1972).

²⁷J. H. Dinan, L. K. Galbraith, and T. E. Fischer, Surf. Sci.

26, 587 (1971); L. K. Galbraith and T. E. Fischer, Surf. Sci. **30**, 185 (1972).

²⁸J. Van Laar and J. J. Scheer, Surf. Sci. **8**, 342 (1967).

²⁹I. Flinn, Surf. Sci. **10**, 32 (1968).

³⁰D. F. Blossey, Phys. Rev. B **2**, 3976 (1970).

³¹D. D. Sell and D. E. Aspnes (unpublished).

³²D. D. Sell, in *Proceedings of the Eleventh International Conference on the Physics of Semiconductors, Warsaw, 1972* (PWN-Polish Scientific Publishers, Warsaw, 1972); and unpublished results.

³³J. A. Rossi, C. M. Wolfe, G. E. Stillman, and J. O. Dimmock, Solid State Commun. **8**, 2021 (1970).

³⁴D. Bimberg and H. J. Queisser, in Ref. 32.

³⁵R. Dingle (unpublished).

³⁶E. H. Bogardus and H. B. Bebb, Phys. Rev. **176**, 993 (1968). However, these authors point out that their data also are consistent and, in fact, are more easily accounted for, with a neutral-donor-free-hole assignment of the 1.5133-eV luminescence.

³⁷J. Shah, R. C. C. Leite, and R. E. Nahory, Phys. Rev. **184**, 811 (1969).

³⁸D. E. Hill, Phys. Rev. B **1**, 1863 (1970).

³⁹D. Bimberg, M. Sondergeld, and E. Grobe, Phys. Rev. B **4**, 3451 (1971).

⁴⁰J. A. Rossi, C. M. Wolfe, and J. O. Dimmock, Phys. Rev. Lett. **25**, 1614 (1970), and references therein.

⁴¹M. A. Gilleo, P. T. Bailey, and D. E. Hill, Phys. Rev. **174**, 898 (1968); Phys. Rev. B **3**, 3581E (1971).

⁴²R. C. C. Leite, J. Shah, and J. P. Gordon, Phys. Rev. Lett. **23**, 1332 (1969).

⁴³Y. Toyozawa, Prog. Theor. Phys. **12**, 111 (1959).

⁴⁴W. C. Tait and R. L. Weiher, Phys. Rev. **178**, 1404 (1969).

⁴⁵W. C. Tait and R. L. Weiher, Phys. Rev. **166**, 769 (1968).

⁴⁶We have observed luminescence from one face of a 10- μ m-thick sample that was optically pumped with a He-Ne laser at the opposite face.

⁴⁷E. Gross, S. Permogorov, V. Travnikov, and A. Selkin, Solid State Commun. **10**, 1071 (1972).

⁴⁸C. Benoit a la Guillaume, A. Bonnot, and J. M. Debever, Phys. Rev. Lett. **24**, 1235 (1970).

⁴⁹G. F. Koster, J. O. Dimmock, R. G. Wheeler, and H. Statz, *Properties of the Thirty-Two Point Groups* (MIT Press, Cambridge, Mass., 1963).

⁵⁰D. W. Langer, R. N. Euwema, K. Era, and T. Koda, Proc. R. Soc. B **2**, 4005 (1970).

⁵¹F. H. Pollak and M. Cardona, Phys. Rev. **172**, 816 (1968).

⁵²M. A. Gilleo, P. T. Bailey, and D. E. Hill, J. Lumin. **1/2**, 562 (1970).

⁵³S. Sakoda and Y. Onodera, J. Phys. Chem. Solids **32**, 1365 (1971).